Parametric Study and Uncertainty Quantification of the Nonlinear Modal Properties of Frictional Dampers

Yekai Sun, Jie Yuan, Luca Pesaresi, Enora Denimal, Loic Salles

Parametric Study and Uncertainty Quantification of the Nonlinear Modal Properties of Frictional Dampers

Yekai Sun
Department of Mechanical Engineering
Imperial College London
London, UK
Email: ys5113@imperial.ac.uk

Jie Yuan*, Luca Pesaresi, Enora Denimal, Loïc Salles
Department of Mechanical Engineering
Imperial College London
London, UK

Abstract *A numerical methodology is described to study the influence of the contact location and contact condition of friction damper in aircraft engines. A simplified beam model is used to represent the blade for the preliminary design stage. The frictional damper is numerically analysed based on two parameters, contact angle and vertical position of the platform. The nonlinear modal analysis is used to investigate the nonlinear dynamic behaviour and damping performances of the system. Harmonic balanced method with continuation technique is used to compute the nonlinear modes for a large range of energy levels. Using such a modelling strategy, modal damping ratio, resonant amplitude and resonant frequency are directly and efficiently computed for a range of design parameters. Monte Carlo simulations together with Latin hypercube sampling is then used to assess the robustness of the frictional damper, whose contact parameters involve much uncertainties due to manufacturing tolerance and also wear effects. The influences of those two parameter are obtained and the best performances of the frictional damper can be achieved when the contact angle is around* 25°-30°. *The vertical position of the platform is highly mode-dependent and other design considerations need to be accounted. The results have been proved that the uncertainties involved contact surfaces do not have significant effects on the performance of frictional damper.*

1 Introduction

The gas turbine engine becomes lighter and more efficient due to the requirements in aerospace industry. The design of many components within the engines, such as turbine bladed disks, approaches their structural limits. Turbine bladed disks are highly loaded during the operation, which undertakes high thermal stress, centrifugal stress and vibrational stress. Large vibrational stress through resonance has a great probability to cause high cycle fatigue , which is one of the most common failure of bladed disks within aircraft engines [1]. The bladed disks have a high modal density and wide range of operating speed makes it impossible to avoid all the critical resonances. Therefore, it is vital to reduce the amplitude around the resonance. In bladed disks, the material damping and aerodynamic damping do not contribute significantly, external damping source is usually required. Because of the highly loaded operating environment, different damping techniques successfully used in other fields cannot work well for bladed disks. Therefore, various of dry frictional dampers are widely used in turbomachinery industries. The major disadvantage is the cost of wear effects between the contact surfaces during the operation of the aeroengine [2].

Different types of dry friction dampers for bladed disks have been explored by many researchers in literature [2, 3]. Friction damping can be introduced in different locations, such as at the root, the tip shrouds or under the platforms as represented Fig.1. Underplatform Dampers (UPD) are one of the most effective friction dampers, it consists of a small piece of metal device and is hold to the underside of platforms between two adjacent blades. The cost of UPDs are relatively low, because they are easy to manufacture, install and replace. Many researchers have made great efforts in analysing the dampers in both numerical simulation and experimental work [4, 5]. Panning et al. [6, 7] have exploited in the regime of dampers optimization for cylindrical and

*Address all correspondence for other issues to this author.

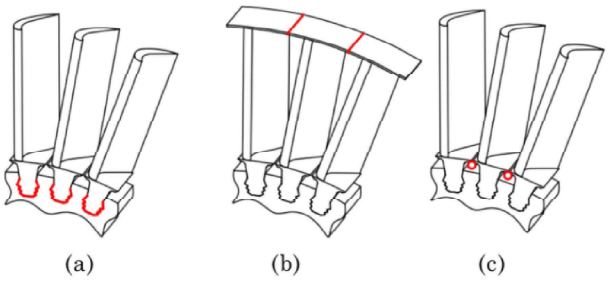

Fig. 1: Common frictional dampers: (a) Root Joints; (b) Tip Shrouds; (c) Underplatform Damper [2]

wedge shaped dampers. The parametric design of asymmetric UPDs have been investigated to avoid the clamped damper between the adjacent blades [8,9]. Most of the previous work are focused on the geometric design of the friction dampers. The vertical position of the UPDs are also important in terms of the damping performances. Beside that, Panning et al. [7] pointed out that the contact angle is expected to be taken into consideration. Hence, the first objective of this proof-of-concept work is to explore the effects of the vertical position of the platform and of the contact angle on the damping performances for UPD.

Structures with frictional contact exhibit a strong nonlinear dynamic behaviour. Different methodologies can be used to compute the steady state solutions of such nonlinear system. Harmonics Balance Method (HBM) is one of the most common frequency domain methods in literature [10]. HBM is a well-established method and many researchers have improved HBM using different methods [11, 12]. HBM in conjunction with continuation technique is widely employed for most of the modelling analysis for nonlinear structural dynamic problem. Continuation technique is the method used for parametric study to evaluate the effects of a specific chasing parameter on system behaviour [13]. HBM integrated with continuation technique are the methodolog used in this work to solve the nonlinear dynamic equation.

Nonlinear modes are defined as an autonomous response for a nonlinear system. Nonlinear Modal Analysis (NMA) is regarded as an effective method to investigate the modal characteristics of amplitude-dependent nonlinear system regarding to resonant frequency, modal damping properties, stiffening/softening effect and modal interaction [2]. In a nonlinear system, superposition and orthogonality conditions are not valid. Therefore, the computation of nonlinear modes is complicated especially in non-conservative system. The first definition of nonlinear mode is given by Rosenberg [14] as a vibration unison[1]. However, this definition cannot be used to explain the internal resonance. Shaw and Pierre [15] proposed nonlinear modes as an invariant manifold, which is mainly used in conservative system. Laxalde et al. [16] proposed a concept of complex nonlinear modes (CNM), which can be extended to a dissipative system, where the solutions are not periodic. Krack [17] further developed a numerical method, namely Extension of Periodic Motion Concept (EPMC), to compute the CNM as a periodic solution in a dissipative system, e.g. system with frictional damper. In EPMC, an artificial damping is applied to compensate the energy change due to friction. A recent published paper differences CNM and EPMC and the corresponding results are addressed [18]. Theoretically, both methods can provide similar results. A periodic solution is better to capture the behaviour of the system with external excitation [2]. Furthermore, both HBM and shooting method can be simply applied to compute the nonlinear modes based on the periodic definition. In this work, EPMC is selected as the numerical method for NMA.

Finally, the modelling of the contact is a complicated task and to be more accurate, the uncertainties associated to the contact roughness that comes from the wear and the manufacturing tolerances must be considered. Therefore, the uncertainty analysis is important to yield an optimal design which is supposed to be robust to the variation of these uncertainties. Many researchers have investigated the uncertainties involved in dynamic analysis for bladed disk [19–21]. A classic method to propagate the uncertainty is the use of Monte Carlo Simulations (MCS) [22]. MCS method is limited for its slow convergence, which requires large number of samples leading to heavy computational cost. Apart from MCS, other methods could be considered for propagation of uncertainty, such as Polynomial Chaos Expansion [23], Kriging [24] and Support-Vector Machine [25]. In these methods, a mathematical approximation is obtained based on a small number of evaluations of the entire system. A lower computational costs can be achieved by using these surrogate models, but a proper validation is expected and convergence issues may appear for high dimension problems. Despite the lower convergence rate, the MCS methods are well known for its robustness regardless of the dimension. The low computation time of the present study makes the MCS conceivable. To improve the convergence of MCS, advanced sampling methods are introduced, such as Quasi-Monte Carlo simulation and structured sampling techniques [26]. One famous method is based on Latin Hypercube Sampling (LHS) and gives a faster convergence rate [27]. Therefore, MCS in corporation with LHS is used in Uncertainty Quantification (UQ) to evaluate the effects of uncertainties within the contact surfaces.

In this work, the influence of the position of the platform and of the contact angle between the damper and the platform are investigated for turbine blades by using NMA. A beam model is used as the reference model to represent the blade in the preliminary design stage. Two design parameters are used to describe the design space of the friction damper, namely the vertical position of the platform and the contact angle. Nonlinear modes and modal characteristics are computed through HBM in conjunction with continuation technique. Resonant frequency and modal damping ratio are calculated through the analysis to evaluate the damping performances. Then, the uncertainties associated to the contact parameters are taken into consideration to identify a robust configuration of the damper. This paper is organized

[1] Vibration unison: where all points in a structure reach their equilibrium position and their extreme position simultaneously [14]

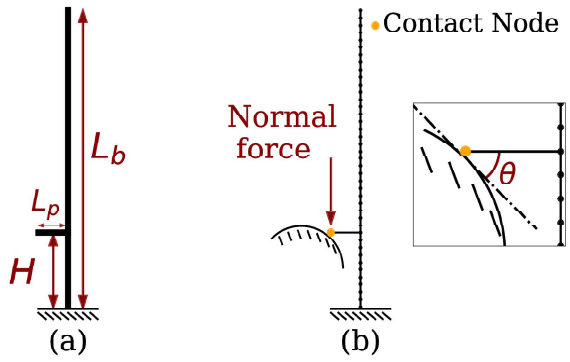

Fig. 2: Mechanical model: (a) Two dimensional view X-Y Plane; (b) Two dimension finite element model

as follows: a detailed description of the mechanical models used is introduced in Section 2. After that, numerical formulations are briefly explained in Section 3. Performances of the damper are then explored for a wide range of chosen design parameters in Section 4. Finally, in Section 5, the robustness of friction damper is further assessed using the UQ techniques followed by the conclusions.

2 Model Description

The objective of the present study is to investigate the influences of the position of the damper and contact angle of the UPD in terms of its capacity to dissipate energy. The mechanical model and contact model used in this work is described in this section.

2.1 Mechanical Model

The model used in this work is based on a simple 2D model represented Fig.2a. The blade is modelled with a beam of length L_b, on which one platform is fixed at the height H, where $H/L_b \in (0,1]$. The latter is modelled with a beam of length L_p. This modelling choice has been widely used in the numerical and experimental analysis in literature [4]. Firstly, several simplifications were made about the model shown in Fig.2a and listed below.

1. *Blade and platform:* The properties of the blade and platform are assumed to be constant along the axis of rotation. Therefore, the blade structure is considered as a two dimensional Finite Element (FE) model. In addition, the turbine blade in turbomachinery are rigid enough to avoid the kinematic nonlinearities. Therefore, a linear Euler-Bernoulli beam element with bar element is used to model the flexural and axial vibration of the blade-platform. To understand the influences of the contact angle, only one side of the damper (usually UPDs are placed underside of the adjacent blades) is modelled.
2. *Cyclic symmetry:* Cyclic symmetry boundary condition is usually required for the actual design of UPD. However, to investigate the impact of these factors (vertical position of the damper and contact angle), the cyclic symmetric framework is not considered so that each blade is isolated.
3. *Damper:* A cylindrical damper is considered, because it is inexpensive to test for different contact angles in the future experimental work as shown in Fig2b. The damper is assumed as a rigid body and completely fixed to the ground so the contact force is introduced between the tip of the platform and ground. Therefore, the influences of the contact angle can be obtained independently.
4. *Frictional contact:* Only one contact node is taken into account, which is used to model the line contact for the cylindrical damper. The effect of micro-slip is also considered for this work. The normal force applied to the contact surface is used to simulate the centrifugal force for real bladed disks.

A simplified model is shown in Fig.2b. The platform can be located between the bottom and the tip of the blade to test the different vertical positions of the UPD. The contact interface between the damper and the blade is modelled with a contact point at the tip of the platform. The angle θ between the damper and the platform is taken in $[0,\pi/2]$. If $\theta = 0$, then the local contact force is purely friction, whereas if $\theta = \pi/2$ there is only impact between the contact points. A constant vertically downwards normal force N is applied at contact node to represent the reaction force from the centrifugal effect due to the rotation of the bladed disk. This force is always positive and N is set to be 50 N.

For 2D FE beam model, each node has three Degrees of Freedom (DOFs) which are the translational DOFs in X-Y plane and a rotational one. The beams have the following dimensions: a length of 200 mm, a width of 40 mm and a thickness of 3 mm, which is the same beam used in [28]. The mass and stiffness matrices of each element can be obtained as in [29]. A fixed interface component mode synthesis method, namely the Craig-Bampton method [30], is used to reduce the computational cost [31].

2.2 Contact Model

The physical phenomenon of frictional contact is complicated in a tribological problem. A proper contact model is expected to consider many factors involved in contact surfaces, such as adhesive wear, roughness of the surface and fretting [32, 33]. To consider these tribological properties, the contact model is needed to link the contact parameters to the micro-mechanics of the frictional contact. Using such contact model gives an insight description of the physical behaviour of the friction. In the present study, a 2D cylindrical damper with a point contact is modelled. A simplistic contact model is used to calculate the nonlinear dynamic response in a fast time scale [34] and is represented in Fig.3. This contact model consists a Jenkins element and a unilateral spring. In the normal direction, unilateral-elastic behaviour with a stiffness k_n and a preload N is considered. Whereas, in the tangential direction elastic dry Coulomb friction with the coefficient μ and a stiffness k_t is considered. $\mathcal{W}(t)$ is the internal variable representing the sliding position during a vibration

cycle. The value of the friction coefficient μ is chosen as 0.5. The dynamic friction coefficient is assumed to be identical to the static one. The values of contact stiffness is selected as the same value in [28].

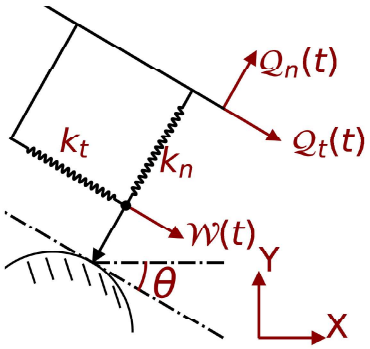

Fig. 3: Two dimensional contact model

3 Numerical Methods

The mechanical model as well as the modelling choices have been presented in Section 2. The objective of this section is to describe the different numerical techniques used for the computation of the dynamic response of the system. Hence, at the first place, HBM is described. Then the continuation technique is presented.

The nonlinear modes are considered as the free vibration solutions of an autonomous system with nonlinear force. The dynamic equation for such system can be expressed as Eqn.(1), where $\underline{\underline{\mathbf{M}}}$, $\underline{\underline{\mathbf{K}}}$ are mass and stiffness matrices respectively. $\underline{Q}(t)$ is the generalized displacement vector. $\underline{\mathcal{F}_{nl}}(\underline{Q})$ corresponds to the friction forces determined with the model given in Section 2.2.

$$\underline{\underline{\mathbf{M}}}\,\underline{\ddot{Q}} + \underline{\underline{\mathbf{K}}}\,\underline{Q} + \underline{\mathcal{F}_{nl}}(\underline{Q}) = 0 \tag{1}$$

The EPMC approach is used to compute the nonlinear modes. To obtain the periodic solution, a negative artificial mass-proportional damping is introduced into the system to compensate the energy loss due to friction [17]. The artificial damping matrix $\underline{\underline{\hat{\mathbf{C}}}}$ is: $\underline{\underline{\hat{\mathbf{C}}}} = -2\omega_0\zeta\underline{\underline{\mathbf{M}}}$, where ω_0 is resonant frequency and ζ is modal damping ratio. Therefore, the external damping generated by frictional contact can be represented as the modal damping ratio ζ. In NMA, the mode shapes, resonant frequency and modal damping ratio vary with the energy level of the mode. Therefore, a modal amplitude α is introduced into the system to represent the energy level of the mode. Thus, the dynamic equation of the system becomes:

$$\alpha\underline{\underline{\mathbf{M}}}\,\underline{\ddot{Q}} + \alpha\underline{\underline{\hat{\mathbf{C}}}}\,\underline{\dot{Q}} + \alpha\underline{\underline{\mathbf{K}}}\,\underline{Q} + \underline{\mathcal{F}_{nl}}(\alpha\underline{Q}) = 0 \tag{2}$$

3.1 Harmonic Balance Method

The method used for numerical analysis is an existing HBM with Alternating Frequency/Time (AFT) and has been discussed in details in [12,35]. The nonlinear dynamic equation Eqn.(2) is solved in the frequency domain. Since the response of system is periodic, the variables that depend of the time are decomposed by a Fourier series truncated at the harmonic N_H. In the present study, the odd number of harmonics up to the 7th are considered in the simulation and 2^8 samples for each period are used in the AFT. Hence, the displacements $\underline{Q}(t)$ can be written as :

$$\underline{Q}(t) = \sum_{p=0}^{N_H} \text{real}\left\{\underline{\tilde{Q}}_p \times [\cos(p\omega_0 t) + i\sin(p\omega_0 t)]\right\} \tag{3}$$

where $\underline{\tilde{Q}}_p = \underline{\tilde{Q}}_p^c - i\,\underline{\tilde{Q}}_p^s$ is the cosine and sine terms associated to the harmonic p. When Eqn.(3) is inserted into Eqn.(2) and all properties in time domain are decomposed by Fourier series with Galerkin projection, the dynamic equation in frequency domain is obtained as Eqn.(4).

$$\underline{\underline{\mathbf{A}}}(\omega_0,\zeta) \times \alpha\underline{\tilde{Q}} + \underline{\tilde{\mathcal{F}}_{nl}}(\alpha\underline{\tilde{Q}}) = 0 \tag{4}$$

where $\underline{\underline{\mathbf{A}}}(\omega_0,\zeta)$ is the dynamic stiffness matrix, $\underline{\tilde{Q}}$ is the collection of Fourier coefficients of the displacement vector $\underline{\tilde{Q}} = [\underline{\tilde{Q}}_{p=0}, \underline{\tilde{Q}}_{p=1}, \cdots, \underline{\tilde{Q}}_{p=N_H}]^{\mathrm{T}}$, $\underline{\tilde{\mathcal{F}}_{nl}}(\alpha\underline{\tilde{Q}})$ is vector of nonlinear forces. The nonlinear forces in frequency domain are computed based on AFT and readers can refer [12] for further details. The problem given by Eqn.(4) is underdetermined since there are three more unknowns than the number of equations, hence three extra constraints are necessary to solve the problem. The first constraint is given by the mass normalization that ensures a positive modal amplitude α as shown in Eqn.(5). The second constraint is given by the phase normalization in Eqn.(6), since absolute phase is arbitrary in autonomous system. The last constraint is given by the corrector used in the continuation process and is discussed in the next section.

$$\underline{\tilde{Q}}^{\mathrm{T}} \cdot \underline{\underline{\mathbf{M}}} \cdot \underline{\tilde{Q}} - 1 = 0 \tag{5}$$

$$\text{imag}(\tilde{Q}_p^1) = 0 \tag{6}$$

3.2 Continuation Method

In NMA, the characteristics of a nonlinear modes depend on the modal amplitude α. The continuation method can be used to obtain the evolution of dynamic behaviour of the system for a range of the modal amplitude α. In a standard continuation procedure, each iteration can be characterised into two steps: prediction and correction. Readers can refer to [13] for a detailed description and numerical formulation of continuation process. In the present study, a secant predictor and an arclength corrector is used.

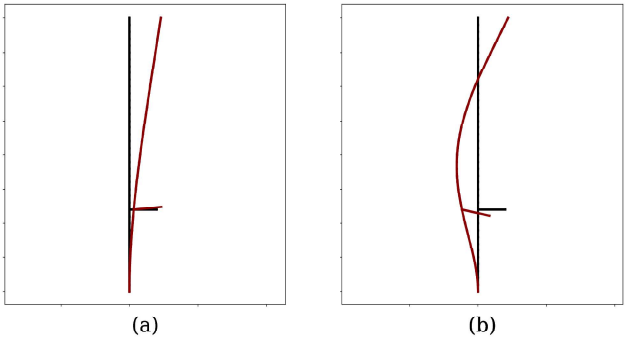

Fig. 4: Linear modeshape for beam model: (a) 1^{st} Bending mode $\omega_0 = 391.8\ rad/s$; (b) 2^{nd} Bending mode $\omega_0 = 2333.1\ rad/s$

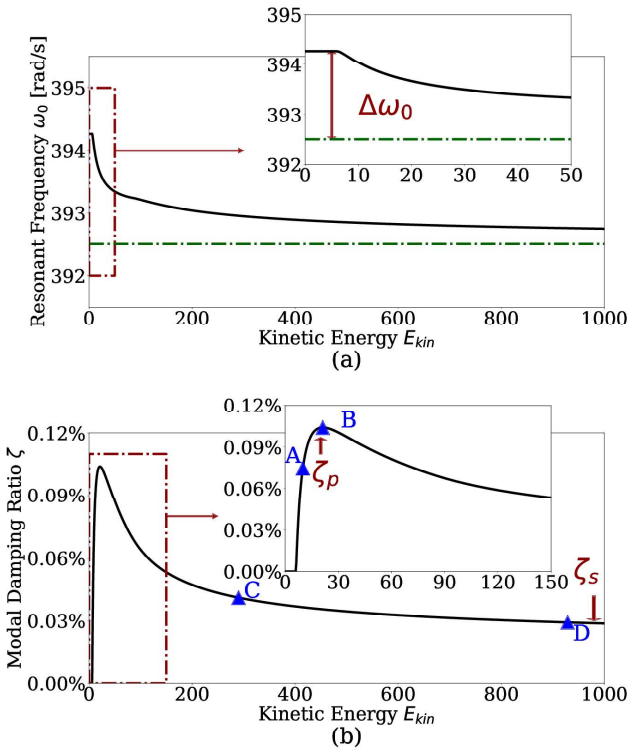

Fig. 5: Modal characteristics against kinetic energy ($H/L_b = 0.3$ and $\theta = 25^\circ$): (a) Resonant frequency; (b) Modal damping ratio

4 Numerical Results

This section is devoted to the discussion of the results. Firstly, a specific configuration of the system is presented to characterize the performances of the damper and to illustrate the results obtained based on the methodology presented previously. Then the performances of the frictional damper are analysed for all the possible configurations of the system.

4.1 Nonlinear Modal Analysis

In this part, a specific configuration of the system is considered where the position of the platform is characterized by $H/L_b = 0.3$ and the contact angle θ is set to 25°. At the first place, the first two linear modes are determined, as shown in Fig.4. It corresponds to the first two bending modes at 391.8 rad/s and 2333.1 rad/s. The 1^{st} bending mode is chosen to illustrate the damping performances. The methodology presented in the previous section is applied and for a range of modal amplitude α. The periodic solution $\underline{Q}(t)$ and modal properties, including the resonant frequency ω_0 and the modal damping ratio ζ, are computed. The modal properties are illustrated respect to kinetic energy instead of modal amplitude. Since the total kinetic energy varies during the oscillation, the mean kinetic energy per period E_{kin} is calculated based on Parseval's theorem [28]. Results are shown Fig.5, where the evolution of the resonant frequency ω_0 and the modal damping ration ζ are given versus the kinetic energy E_{kin}. The resonant frequency ω_0 is constant and equal to 394.2 rad/s when the kinetic energy E_{kin} is inferior to 8, and then it decreases and stabilizes at 392.6 rad/s when the higher level of kinetic energy is achieved. The natural frequency of the 1^{st} bending mode is also shown as the green dotted line in Fig.5a. This variation of the resonant frequency with respect to the kinetic energy is typical to a structure with frictional contact. Looking at the evolution of modal damping ratio ζ (see Fig.5b), important variations are also observable. Principally, when kinetic energy E_{kin} is lower than 8, the modal damping ratio is null. Then it increases to reach a maximum values ζ_p equals to 0.1% when kinetic energy E_{kin} reaches around 20. Finally, it decreases and tends to 0.025%.

When the kinetic energy E_{kin} is smaller than 8, the contact mode is sticking and the whole system is purely linear, so the resonant frequency ω_0 of the system remains constant and there is no energy loss due to the friction. The contact points start to slide when kinetic energy E_{kin} is equal 8. The resonant frequency decreases due to the softening effect caused by friction (sliding). The total change of resonant frequency is named as $\Delta\omega_0$, which indicates the shift in resonant frequency compared to the baseline configuration (no damper).

The performances of the damper can be directly assessed through Fig.5b. The maximum modal damping ratio ζ_p can be directly obtained in the figure. However, when modal damping ratio at its maximum value ζ_p, a small change in kinetic energy results in a dramatic decrease of the modal damping ratio. Whereas, the analysis demonstrates the presence of steady region when the kinematic energy is larger (i.e. $E_{kin} > 600$). Indeed, the damping is not very sensitive to a variation of the kinetic energy and reaches a non-zero asymptotic value when kinetic energy E_{kin} is further increased. This asymptotic value of modal damping ratio is named as ζ_s, which is approximated from the simulation. To further demonstrate the energy dissipated, four normalised hysteresis loops for different levels of kinetic energy are given Fig.6. The corresponding levels of amplitude are represented Fig.5b with the blue points. Thus, Fig.6a shows the normalised hysteresis loop before the maximum modal damping ratio ζ_p is achieved (example A). The normalised hysteresis loop at ζ_p (example B) is given in Fig.6b.

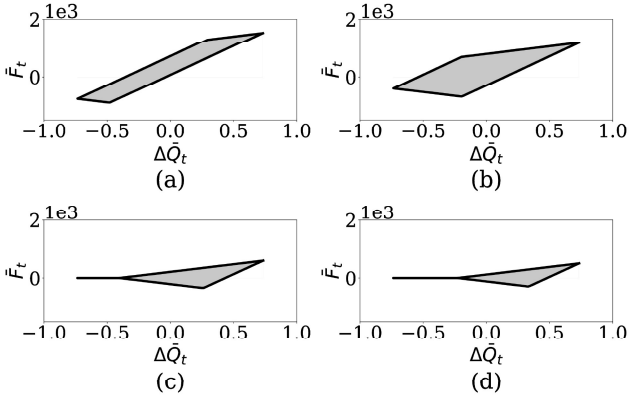

Fig. 6: Normalised hysteresis loops for example point in Fig5b: (a) Example A; (b) Example B: maximum modal damping ratio ζ_p; (c) Example C; (d) Example D: asymptotic value of modal damping ratio ζ_s

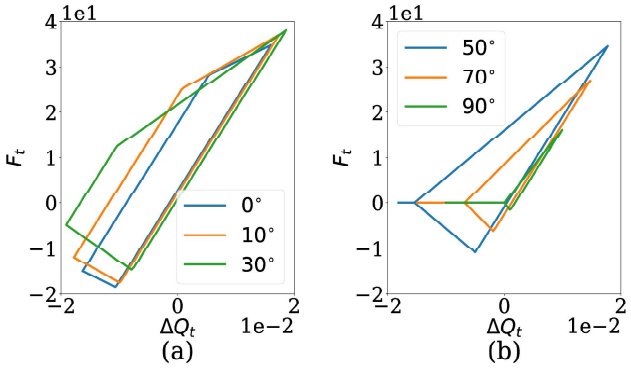

Fig. 7: Hysteresis loop for different contact angle θ: (a) θ = 0°, 10° and 30°; (b) θ = 50°, 70° and 90°

The other two hysteresis loops (example C and D) in Fig.6 correspond to higher values of the kinetic energy where the damping reach its asymptotic value. Before the maximum damping is reached, the hysteresis loop is a quadrilateral, so the damper and the platform are always in contact and friction occurs. Whereas after the maximum damping ratio, loss of contact occurs.

4.2 Design Space Exploration

In the previous part, a specific case was presented to illustrate the nonlinear dynamic behaviour of the blade with cylindrical frictional damper. In addition, parameters of interest for damper design are also defined. In the present part, the performances of the damper are determined for all possible positions H/L_b of the platform and all contact angles θ. Hence, the three performance indicators, namely ζ_p, ζ_s and $\Delta\omega_0$ (see Fig.5), are determined for the 1^{st} and the 2^{nd} bending modes of the system. The linear modeshape of the baseline configuration (no damper) for first two bending modes are displayed Fig.4.

The results are shown Fig.8. The figures in the left column correspond to the results associated to the 1^{st} bending mode, and the right column to the 2^{nd} bending mode. For each mode, the maximum modal damping ratio ζ_p, the asymptotic value of modal damping ratio ζ_s and the shift of resonant frequency $\Delta\omega_0$ are given. The first obvious observation is that the three parameters are highly related to both design parameters, namely the vertical position of platform and contact angle.

By looking at the evolution of modal damping ratios (see Fig.8(a,b,d,e)), it appears that the maximum is always achieved when the platform is close to the top of the blade. This can be explained by the fact that if the platform locates at the bottom of the blade, so where the relative displacement between contact nodes are small, it will be more difficult to initiate sliding and so less energy is dissipated by the contact leading to lower modal damping ratio. This is confirmed by the evolution of the modal damping ratios for the 2^{nd} bending mode. Larger displacement can be achieved at an intermediary position of the platform, and so an increase of the damping ratios are also observable when the platform is located around the middle of the blade.

The contact angle θ has also an crucial impact on the damping performances. It appears that the damping ratios and the frequency shift have higher values when the angle is smaller. To illustrate the influences of the contact angle, the hysteresis loop for different contact angles and when $H/L_b = 0.3$ is plotted in Fig.7. The area enclosed by a closed hysteresis loop represents the total energy dissipated due to friction. For values of θ inferior to 30°, the peak-to-peak value of F_t decreases but the displacement variations increase, which leads to an increase of the enclosed area (see Fig.7a). When θ is superior to 50° (see Fig.7b), then loss of contact occurs and the enclosed area decreases. Further increase θ, the energy dissipated by friction decreases. In the case of θ = 90°, the contact mode is separating-sticking and there is no energy loss due to sliding, so three objectives tend to zero. From Fig.8b, the maximum case of the ζ_s for the 1^{st} bending mode is achieved while contact angle θ is around 25°-30°. For the 2^{nd} bending mode, from Fig.8d and Fig.8e, best performances of the damper are also obtained when the contact angle is within 25°-30°.

The shift of resonant frequency for both modes are shown in Fig.8c and Fig.8f. The evolution of resonant frequency shift is similar to the evolution of the modal damping ratios, which leads to similar analysis. The contour plots in Fig.8c and Fig.8f shows the percentage of variation of frequency ($\Delta\omega_0/\omega_0$). The maximum shift of resonant frequency for the 1^{st} and the 2^{nd} bending modes are 12% and 0.3% respectively. It is obvious to find out that the frequency shift for the 2^{nd} bending mode is smaller than for the 1^{st} mode in term of both actual shift of resonant frequency and percentage. The shift of resonant frequency is caused by softening effects due to the sliding on contact interfaces. For different modes and different H/L_b, the natural frequency sensitivities with regards to contact stiffness ($\partial\omega_0/\partial k$, $k = k_n = k_t$) are different. Therefore, sensitivity analysis are used to investigate the effect of the contact stiffness on the natural frequency. Natural frequency sensitivities are calculated. The sensitivity for the first three natural frequencies for different

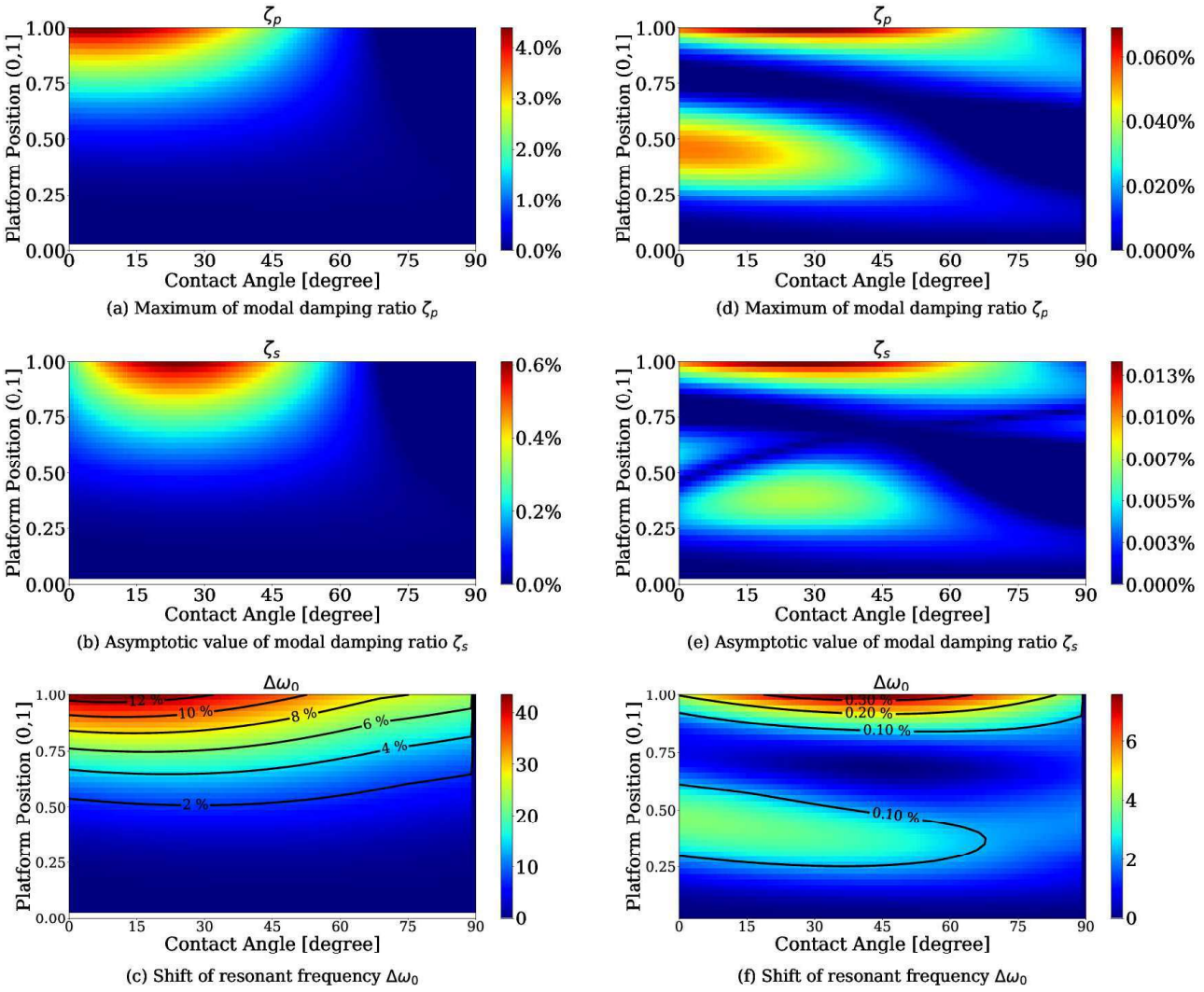

Fig. 8: Three design objectives (ζ_p, ζ_s and $\Delta\omega_0$): (a, b , c) 1^{st} Bending mode; (d, e, f) 2^{nd} Bending mode

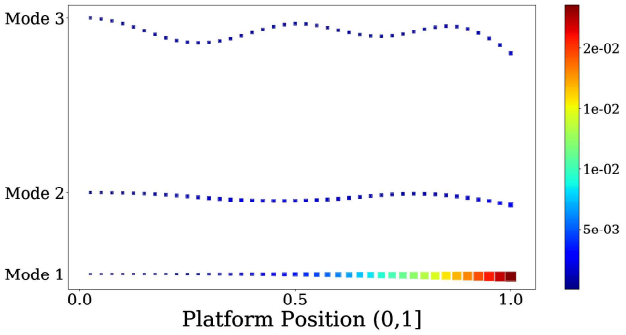

Fig. 9: Natural frequency sensitivity

platform positions are shown in Fig.9. It is easy to find out the natural frequency of the 1^{st} bending mode is more sensitive to the contact stiffness. In addition, the sensitivities are also increased with the value of H/L_b. The shift of resonant frequency is an important factor for the design of the damper. Indeed, the damper is designed to get a certain resonance frequency shift, but a significant change in frequency can cause interaction with other modes.

Table 1: Uncertain Parameters

	Mean	Standard deviation
Friction coefficient μ	0.5	0.05
Contact stiffness k	2 N/mm	0.1 N/mm

The damping performances are very sensitive to the mode shape and the displacement at the contact nodes. The best configuration for the damper depends on the considered mode. By considering the 1^{st} bending mode, the best configuration would be a vertical position of $H/L_b = 1$, whereas for the second mode $H/L_b = 0.3$ is the optimal position. Except the damping performance, other design considerations also need to be accounted, e.g. placing damper at mid-span might have detrimental effect on aerodynamic performance.

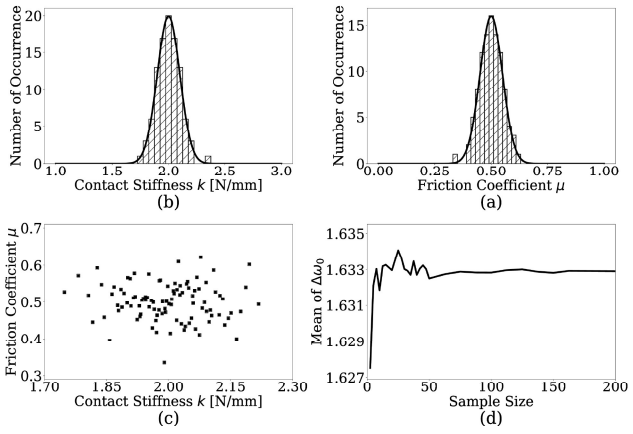

Fig. 10: UQ: (a) Number of occurrence for contact stiffness; (b) Number of occurrence for friction coefficient; (c) Samples from LHS; (d) Example of convergence study

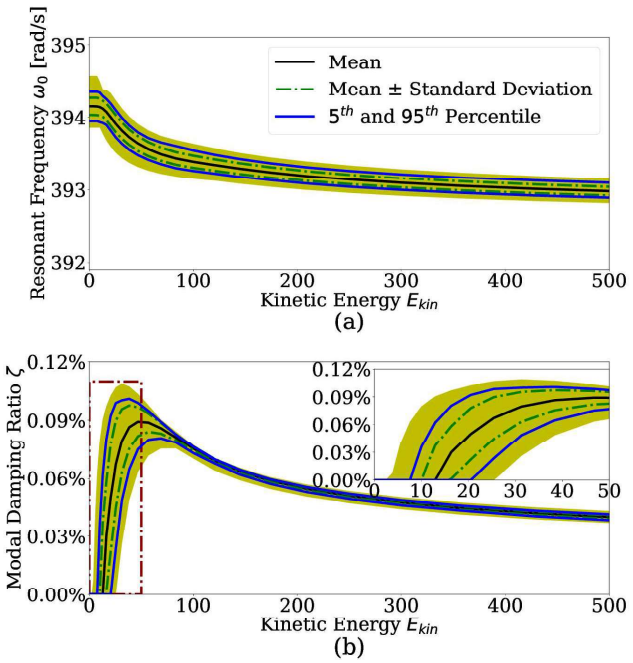

Fig. 11: MCS: Stochastic modal characteristics against kinetic energy ($H/L_b = 0.3$, $\theta = 25°$): (a) Resonance frequency; (b) Modal damping ratio

For this reason, industrials give their priority to place the UPD at lower position, which is regarded as the most efficient damping technique to reduce the vibrational stress of bladed disks structure [4].

5 Uncertainty Quantification

The previous section was devoted to the analysis of the damping performances for different configurations of the system. This study has been performed in a deterministic case where all the parameters are supposed to be known and constant. However, some parameters within contact surfaces might be uncertain and have a non-negligible impact on the damper performances. So the objective of this section is to investigate the impact from those uncertainties on the performances of the damper.

Thus, two parameters that define the contact are considered as uncertain and MCS are performed. This choice is motivated by the fact that the roughness of contact surfaces cannot be assumed as a constant due to manufacturing tolerance and wear effect caused during operation. The two contact parameters considered are the friction coefficient μ and the contact stiffness k ($k = k_n = k_t$). A normal distribution law is assumed for both uncertain parameters [19, 20]. The nominal value and standard deviation of the uncertain parameters are given Table 1.

The methodology adopted here to propagate the uncertainty is the classic MCS method. To ensure a quicker converge, the samplings are generated based on Latin Hypercube Sampling (LHS) [27] with an open source software OpenTURNS [36]. A set of 100 sampling is selected after a convergence study as shown in Fig.10d. The distributions and the repartition of the input points are given Fig.10.

For a sake of consistency and according to previous results, only the 1^{st} bending mode is considered for this study. A first case where $H/L_b = 0.3$ and $\theta = 25°$ is considered as an illustration. For all the couples (μ, k) generated based on a LHS by OpenTURNS, the evolution of the stochastic resonant frequency and the modal damping ratio with the kinetic energy E_{kin} are given Fig.11. The mean of each parameter as well as the 5^{th} and 95^{th} percentile are given. For the resonant frequency, a wider band is obtained before the sliding occurs. In this case, the friction force only depends on the contact stiffness. When the kinetic energy E_{kin} is greater than 8, the resonant frequency starts to decrease and the band becomes thinner. The friction force is dominated by friction coefficient instead of contact stiffness. So the contact stiffness has a higher influences on the resonant frequency at low level of kinetic energy, whereas influences of the friction coefficient is important at higher levels of kinetic energy.

Considering the evolution of the modal damping ratio, the two contact parameters have an impact as soon as sliding occurs and changes the threshold at which sliding appears (between 3 and 25). It has also an impact on the maximum of the modal damping ratio (0.11% versus 0.07%) and on the kinetic energy E_{kin} at which it appears (30 versus 80). However, the influences on modal damping ratio is small once loss of contact appears. So performances of the damper are affected by the uncertainties associated to the contact parameters.

To study the impact of these uncertain parameters, the procedure is performed for all the positions of the damper and all the contact angles. The mean and the standard deviation of modal damping ratios ζ_p, ζ_s and the shift of resonant frequency $\Delta\omega_0$ are determined. Results are given in Fig.12. By comparison to deterministic results (see Fig.8), the evolution of the mean of the different parameters does not give a significant difference. Indeed, the configuration which gives optimal damping and the variations of three performance indicators are very similar. For area where no slid-

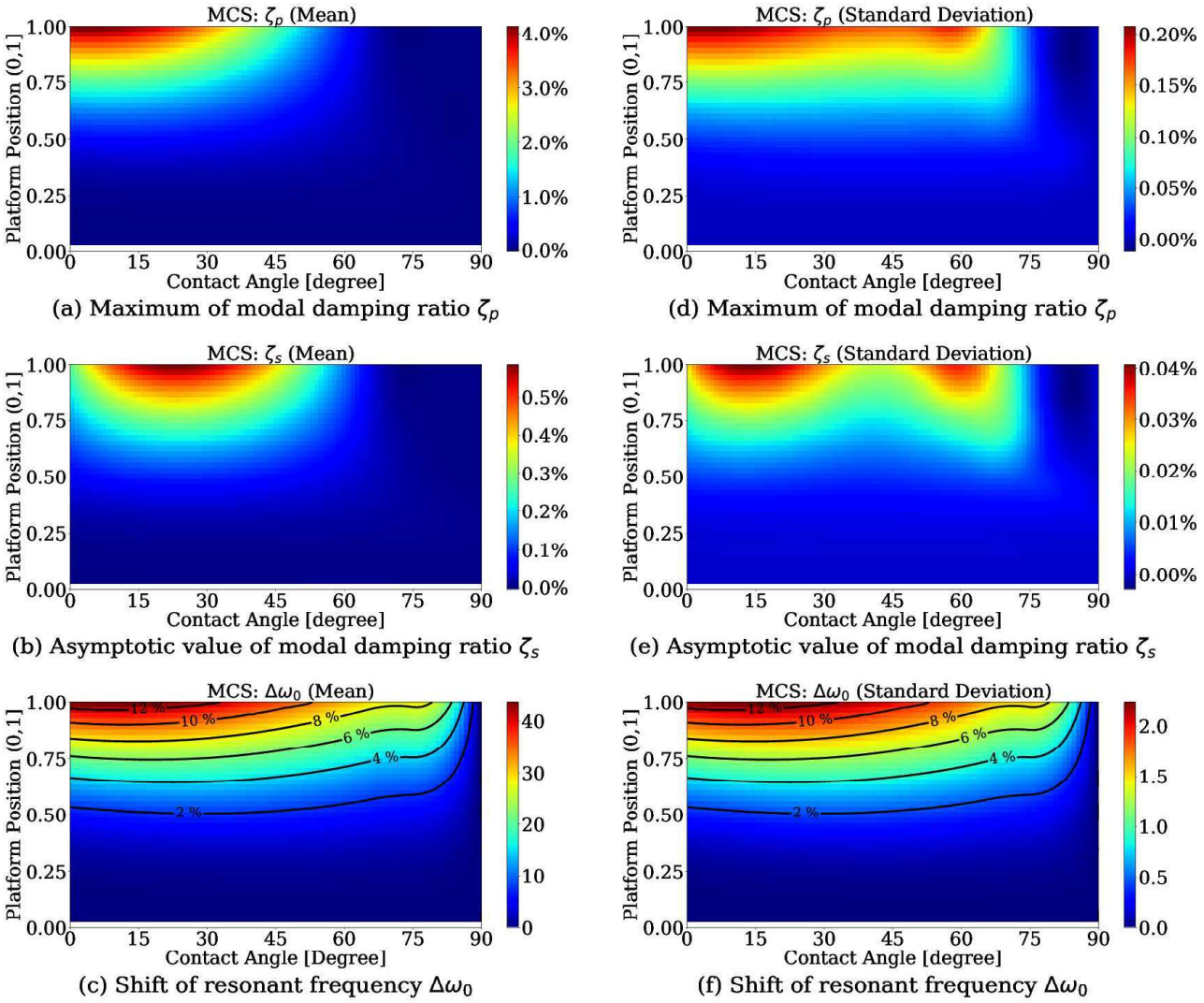

(a) Maximum of modal damping ratio ζ_p (d) Maximum of modal damping ratio ζ_p

(b) Asymptotic value of modal damping ratio ζ_s (e) Asymptotic value of modal damping ratio ζ_s

(c) Shift of resonant frequency $\Delta\omega_0$ (f) Shift of resonant frequency $\Delta\omega_0$

Fig. 12: MCS: Three design objectives (ζ_p, ζ_s and $\Delta\omega_0$): (a, b, c) Mean; (d, e, f) Standard deviation

ing occurs in the dynamics of the system (i.e. $\zeta_p = 0$), this is justified by the fact that those uncertain parameters have no significant influences on ζ (see Fig.11b). So in the area where $\zeta_p = 0$, no variation is expected and so the variance remains close to zero. In the areas, where ζ_p and ζ_s are non-zero, larger variances are observed. As seen in Fig.11b, the value of the maximum modal damping ratio ζ_p is highly influenced by the uncertain parameters, which is confirmed by the high variances. Similarly, the modal damping ratio ζ_s is influenced by the variation of the uncertain parameters, but less variations are observed than for ζ_p (see the wider band for ζ_p than ζ_s on Fig.11b), which is in concordance with the lower level of variance observed for ζ_s compare to those of ζ_p (0.2% versus 0.04%). As for the shift of resonant frequency, the maximum standard deviation for $\Delta\omega_0$ is around 2 rad/s as shown in Fig.12f. By considering the standard deviation of the all three design objectives (ζ_p, ζ_s and $\Delta\omega_0$), it has been proved that the uncertainties involved contact surfaces do not have significant effects on the performance of frictional damper.

6 Conclusion

In summary, a preliminary parametric design of the friction damper for aero-engine turbine blades has been effectively explored using the nonlinear modal analysis. A 2D beam model was used to represent the blade and platform as a case study. Two design parameters, namely the contact interface angle and the vertical position of the platform on the blade, have been considered for the parametric study of the friction damper design. With such a definition of design parameters, the model is able to simulate the dynamics behaviour of different configurations for underplatform damper.

Nonlinear modal anlysis based on the concept of the extension of periodic motions concept for non-conservative system is performed for different configurations. Thanks to the harmonic balance method with continuation technique, resonant frequency and modal damping ratio can be directly and efficiently calculated for a wide range of kinetic energy. The performances of the frictional damper has been assessed based on three objectives: the maximum modal damping ra-

tio, asymptotic limit of the modal damping ratio and the shift of the resonant frequency. The results showed an optimal configuration of the frictional damper can be achieved when contact angle is around 25°-30°. The vertical position of the platform is highly mode-dependent and other design considerations need to be addressed. In nonlinear modal anlysis, it is important to notice that there is non-zero asymptotic limit of the modal damping ratio, which indicates that the frictional damper is able to dissipate the energy at higher level of kinetic energy. Frictional damper is usually designed to mitigate resonance with higher modes and the first several modes are commonly avoided. Since this work is considered as preliminary study for future experimental work. Only the first two bending modes are considered. An effective design of underplatform damper can significantly reduce the maximum dynamic stress, which contribute to a higher fatigue safety factor and ensure the guaranteed high cycle fatigue life.

As the contact parameters on the frictional interface involve much uncertainties due to the manufacturing tolerance and the wear effects on their contact surfaces, they would significantly change the dynamics of the friction damper. To evaluate the robustness of the friction damper subjected to these uncertainties, Monte Carlo simulations together with Latin hypercube sampling is used to quantify the effects of these uncertainties on the modal characteristics of the friction damper. By considering the mean value and standard deviation from uncertainty quantification process, the uncertainties involved contact surfaces do not have significant influence on the performance of friction damper. A convinced experimental work is expected as the validation of the numerical analysis for this blade structure with friction damper.

Acknowledgement

The first author is grateful to China Scholarship Council (File NO. 201708060239) for providing the financial support for this project.

References

[1] Yuan, J., Scarpa, F., Titurus, B., Allegri, G., Patsias, S., and Rajasekaran, R., 2017. "Novel frame model for mistuning analysis of bladed disk systems". *ASME J Vib Acoust,* ***139***(3), p. 031016.

[2] Krack, M., Salles, L., and Thouverez, F., 2016. "Vibration prediction of bladed disks coupled by friction joints". *Archives of Computational Methods in Engineering,* ***24***, pp. 589–636.

[3] Sinha, A., and Trikutam, K. T., 2017. "Optimal vibration absorber with a friction damper". *ASME J Vib Acoust,* ***140***(2), p. 021015.

[4] Pesaresi, L., Salles, L., Jones, A., Green, J. S., and Schwingshackl, C. W., 2017. "Modelling the nonlinear behaviour of an underplatform damper test rig for turbine applications". *Mechanical Systems and Signal Processing,* ***85***, pp. 662–679.

[5] Pesaresi, L., Armand, J., Schwingshackl, C., Salles, L., and Wong, C., 2018. "An advanced underplatform damper modelling approach based on a microslip contact model". *Journal of Sound and Vibration,* ***436***, pp. 327–340.

[6] Panning, L., Sextro, W., and Popp, K., 2000. "Optimization of interblade friction damper design". *ASME. Paper No.2000-GT-0541.*

[7] Panning, L., Sextro, W., and Popp, K., 2002. "Optimization of the contact geometry between turbine blades and underplatform dampers with respect to friction damping". *ASME. Paper No.GT-2002-30429.*

[8] Gastaldi, C., and Gola, M. M., 2016. "Pre-optimization of asymmetrical underplatform dampers". *ASME J Eng Gas Turb Power,* ***139***(1), p. 012504.

[9] Gastaldi, C., Berruti, T. M., and Gola, M. M., 2018. "Best practices for underplatform damper designers". *Proceedings of the Institution of Mechanical Engineers, Part C: Journal of Mechanical Engineering Science,* ***232***(7), pp. 1221–1235.

[10] Krylov, N., and Bogoliubov, N., 1943. *Introduction to Non-linear Mechanics.* Annals of mathematics studies. no.11. Princeton University Press.

[11] Urabe, M., 1965. "Galerkin's procedure for nonlinear periodic systems". *Archive for Rational Mechanics and Analysis,* ***20***(2), pp. 120–152.

[12] Cameron, T. M., and Griffin, J. H., 1989. "An alternating frequency/time domain method for calculating the steady-state response of nonlinear dynamic systems". *ASME J Appl Mech,* ***56***(1), pp. 149–154.

[13] Sarrouy, E., and Sinou, J.-J., 2011. "Non-linear periodic and quasi-periodic vibrations in mechanical systems - on the use of the harmonic balance methods". In *Advances in Vibration Analysis Research*, F. Ebrahimi, ed. InTech, Rijeka, ch. 21.

[14] Rosenberg, R. M., 1960. "Normal modes of nonlinear dual-mode systems". *ASME J Appl Mech,* ***27***(2), pp. 263–268.

[15] Shaw, S. W., and Pierre, C., 1991. "Non-linear normal modes and invariant manifolds". *Journal of Sound and Vibration,* ***150***(1), pp. 170–173.

[16] Laxalde, D., Salles, L., Blanc, L., and Thouverez, F., 2008. "Non-linear modal analysis for bladed disks with friction contact interfaces". *ASME. Paper No. GT2008-50860.*

[17] Krack, M., 2015. "Nonlinear modal analysis of nonconservative systems: Extension of the periodic motion concept". *Computers and Structures,* ***154***, pp. 59–71.

[18] Jahn, M., Tatzko, S., Panning-von Scheidt, L., and Wallaschek, J., 2019. "Comparison of different harmonic balance based methodologies for computation of nonlinear modes of non-conservative mechanical systems". *Mechanical Systems and Signal Processing,* ***127***, pp. 159–171.

[19] Petrov, E. P., 2007. "A sensitivity-based method for direct stochastic analysis of nonlinear forced response for bladed discs with friction interfaces". *ASME. Paper No.GT2007-27981.*

[20] Krack, M., Panning, L., Wallaschek, J., Siewert, C., and

Hartung, A., 2012. "Robust design of friction interfaces of bladed disks with respect to parameter uncertainties". *ASME. Paper No.GT2012-68578*.

[21] Krack, M., Tatzko, S., Panning-von Scheidt, L., and Wallaschek, J., 2014. "Reliability optimization of friction-damped systems using nonlinear modes". *Journal of Sound and Vibration,* ***333***(13), pp. 2699–2712.

[22] Metropolis, N., and Ulam, S., 1949. "The monte carlo method". *Journal of the American Statistical Association,* ***44***(247), pp. 335–341.

[23] Sudret, B., 2008. "Global sensitivity analysis using polynomial chaos expansions". *Reliability Engineering and System Safety,* ***93***(7), pp. 964–979.

[24] Kleijnen, J. P., 2009. "Kriging metamodeling in simulation: A review". *European Journal of Operational Research,* ***192***(3), pp. 707–716.

[25] Cortes, C., and Vapnik, V., 1995. "Support-vector networks". *Machine learning,* ***20***(3), pp. 273–297.

[26] Yuan, J., Allegri, G., Scarpa, F., Rajasekaran, R., and Patsias, S., 2015. "Novel parametric reduced order model for aeroengine blade dynamics". *Mechanical Systems and Signal Processing,* ***62***, pp. 235–253.

[27] McKay, M. D., Beckman, R. J., and Conover, W. J., 1979. "A comparison of three methods for selecting values of input variables in the analysis of output from a computer code". *Technometrics,* ***21***(2), pp. 239–245.

[28] Krack, M., Panning-von Scheidt, L., and Wallaschek, J., 2013. "A method for nonlinear modal analysis and synthesis: Application to harmonically forced and self-excited mechanical systems". *Journal of Sound and Vibration,* ***332***(25), pp. 6798–6814.

[29] Przemieniecki, J., 1985. *Theory of Matrix Structural Analysis*. Dover Civil and Mechanical Engineering. Dover.

[30] Craig, JR., R. R., and Bampton, M. C. C., 1968. "Coupling of substructures for dynamic analyses". *AIAA Journal,* ***6***(7), pp. 1313–1319.

[31] Yuan, J., El-Haddad, F., Salles, L., and Wong, C., 2019. "Numerical assessment of reduced order modeling techniques for dynamic analysis of jointed structures with contact nonlinearities". *ASME. Paper No. GT2018-75303*.

[32] Eriten, M., Polycarpou, A., and Bergman, L., 2011. "Physics-based modeling for fretting behavior of nominally flat rough surfaces". *International Journal of Solids and Structures,* ***48***(10), pp. 1436–1450.

[33] Vakis, A., Yastrebov, V., Scheibert, J., Nicola, L., Dini, D., Minfray, C., Almqvist, A., Paggi, M., Lee, S., Limbert, G., Molinari, J., Anciaux, G., Aghababaei, R., Restrepo, S. E., Papangelo, A., Cammarata, A., Nicolini, P., Putignano, C., Carbone, G., Stupkiewicz, S., Lengiewicz, J., Costagliola, G., Bosia, F., Guarino, R., Pugno, N., Müser, M., and Ciavarella, M., 2018. "Modeling and simulation in tribology across scales: An overview". *Tribology International,* ***125***, pp. 169–199.

[34] Yang, B. D., Chu, M. L., and Menq, C. H., 1998. "Stick-slip-separation analysis and non-linear stiffness and damping characterization of friction contacts having variable normal load". *Journal of Sound and Vibration,* ***210***(4), pp. 461–481.

[35] Petrov, E. P., and Ewins, D. J., 2003. "Analytical formulation of friction interface elements for analysis of nonlinear multi-harmonic vibrations of bladed disks". *ASME J Turbomach,* ***125***(2), pp. 364–371.

[36] Baudin, M., Dutfoy, A., Iooss, B., and Popelin, A.-L., 2015. "Openturns: An industrial software for uncertainty quantification in simulation".